Cholinergic stimulation increases cortical spine formation via local inhibitory circuit

Xueyang Zhao, Yu E. Zhang, Lu Yang, Yang Yang

Abstract

The mammalian neocortex receives extensive cholinergic projections from the basal forebrain. Although it has been shown that acetylcholine (Ach) participates in learning-associated cortical plasticity, it's not clear whether Ach can directly modulate structural changes of cortical synapses. Using *in vivo* two-photon microscopy, we show that optogenetic and chemogenetic stimulation of cholinergic neurons in mouse basal forebrain leads to an increase in spine formation on apical dendrites of layer (L) 5 pyramidal neurons in auditory cortex and posterior parietal cortex, and these newly formed spines follow similar spatial rules as the spontaneously formed new spines. Selective blockage of Ach receptors (AchRs) revealed that nicotinic AchRs, but not muscarinic AchRs, are involved in the stimulation-triggered spine formation. Furthermore, γ-Aminobutyric acid (GABA) transmission is required in this process, indicating that acetylcholine acts through GABAergic connections in promoting spine formation. Together, our findings demonstrate that acetylcholine can induce spine formation in both sensory and higher-order cortices, via activating nicotinic AchRs through GABAergic local circuitry. Our work established a direct link between Ach release and cortical spine formation *in vivo*, and shed light on synaptic mechanisms underlying Ach-associated cortical remapping and learning-induced plasticity.

Introduction

The cholinergic system plays an important role in cognitive functions such as attentional modulation, learning and memory [1]. Cholinergic system consists of the basal forebrain, including nucleus basalis, horizontal limb and lateral nucleus of the diagonal band, and substantia innominata, as well as medial septal, globus pallidus, ventral pallidum, and extension of the amygdala [2]. The cholinergic neurons project broadly to hippocampus, olfactory bulb, thalamus, amygdala and all cortical areas. Cholinergic projections to the cerebral cortex mainly originate from basal forebrain. Acetylcholine release in the rat auditory cortex (ACx) accompanies the auditory conditioning process[3], and depleting ACx-projecting cholinergic neurons could impair learning-induced plasticity [4]. Electrical stimulation of NB paired with auditory stimulation resulted in functional remapping of rat ACx [5-7], and could also induce associative learning [8] and improve auditory perception [9], possibly by changing the excitatory and inhibitory synaptic balance [9, 10].

Nicotinic AchRs (nAchRs) and muscarinic AchRs (mAchRs) are both found in multiple cortical neuronal types[11], including glutamatergic pyramidal neurons and GABAergic interneurons expressing somatostatin, parvalbumin, and vasoactive

intestinal peptide. Activation of nAchRs could induce enlargement of spine heads, spine number and synaptic density in cultured hippocampal neurons [12-14], while activation of mAchRs could lead to reversible formation of filopodia from spine heads [15]. These studies were mainly conducted *in vitro*, and it remains unclear how cholinergic system could participate in modulating the structural plasticity of synapses in the cerebral cortex in *vivo*. In comparison, in the dopaminergic system, it has been shown that inhibition of dopamine receptor 1 facilitates spine elimination, while inhibition of dopamine receptor 2 promotes spine formation *in vivo* [16].

In this study, by stimulating cholinergic neurons using optogenetic and chemogenetic methods, we investigated short-term (4 hours) and long-term (1-2 days) structural plasticity of spines on apical dendrites of pyramidal neurons in the auditory cortex (ACx) and posterior parietal cortex (PPC) in mice using *in vivo* two-photon imaging. We observed significant increase in spine formation within hours of cholinergic stimulation in both cortical areas. In addition, we found that nAchRs, but not mAchRs, are required in the fast spine formation, and Ach release acts through GABAergic synapses to induce spine formation in pyramidal neurons.

Results

Optogenetic activation of cholinergic neurons in basal forebrain induces spine formation in mouse auditory cortex within hours

To locate the source of cholinergic projections to ACx, we injected cholera toxin B-488 (CTB-488) into ACx to retrogradely label ACx-projection neurons (**Fig. 1a, b**). We then used immunostaining of choline acetyltransferase (ChAT) to label cholinergic neurons. We identified ACx-projecting cholinergic neurons throughout the rostral-caudal axis of the basal forebrain (**Fig. 1c**), and found that most dual-labeled neurons are concentrated in the ventromedial globus pallidus (GP) and caudal substantia innominate (SI), the caudal-dorsal and lateral part of basal forebrain (**Fig. 1b**). We then injected a Cre-dependent adeno-associated virus (AAV2/9-CAG-FLEX-EGFP) into SI of ChAT-Cre transgenic mice, in which cholinergic neurons express Cre recombinase, and GFP-labeled axon terminals could be observed in all layers of ACx (**Supplementary Fig. 1a, b**).

For optogenetic activation of ACx-projecting cholinergic neurons, we used two strategies: 1, we crossed ChAT-cre mice with Ai32 (RCL-ChR2) mice, and optically stimulated cholinergic neurons through an implanted fiber using blue laser; 2, we injected Cre-dependent AAV2/8-hSyn-FLEX-chrimsonR-tdTomamto into SI of ChAT-cre mice, and stimulated cholinergic neurons using yellow laser (**Fig. 1d and Supplementary Fig. 2**). The experimental results using these two stimulation strategies are comparable and are combined for data analyses.

To examine how cholinergic stimulation affects the spine dynamics in ACx, we used YFP-H transgenic mice, in which a subset of layer 5 (L5) pyramidal neurons express

EYFP. After implanting a chronic transparent window over ACx, we repeatedly imaged spines on apical dendrites of L5 neurons *in vivo* using two-photon microscopy. Previous work showed that paired sound and electrical stimulation of basal forebrain could induce ACx plasticity [6], so we set up three stimulation protocols: 1, paired tone and optogenetic stimulation (*paired Tone & Opto*); 2, optogenetic stimulation only (*Opto only*); 3, tone only (*Tone only*). For each mouse, 6 imaging sessions were performed. On day 1, the baseline spine turnover was recorded by imaging at a 4-hour interval with no manipulation (NS). On day 2, two imaging sessions were performed before and after a 4-hour stimulation session (S1). To further investigate the effects of repeated stimulation, two more imaging sessions were performed on day 3 before and after a second stimulation session (S2) (**Fig. 1e, f**).

We calculated the percentages of spine formation and elimination by comparing the images obtained before and after NS, S1 and S2. We found that the percentages of new formed spines after S1 are significantly higher compared to those after NS in both paired *Tone & Opto* and *Opto only* groups, but not in *Tone only* group (**Fig. 1g**). Therefore, cholinergic stimulation alone is sufficient to trigger increased spine formation in ACx within hours. A second stimulation session on the following day does not further induce increased spine formation, possibly due to limited cellular resource available in the dendrites. Spine elimination was reduced in Tone & Opto group after S1 and S2, compared to NS (**Fig. 1g**).

Previous work has shown that newly formed spines are more likely to disappear[17]. To investigate whether the cholinergic stimulation-induced new spines are more persistent, we quantified the percentages of newly formed spines that survived over 1 day in all three groups. We found that most new spines disappear after 1 day (**Supplementary Fig. 3a)**. Therefore, cholinergic stimulation-induced new spines are as susceptible to elimination as spontaneously formed new spines.

Chemogenetic activation of cholinergic neurons in basal forebrain induces spine formation in mouse auditory cortex within hours

In addition to optogenetic stimulation, we used the designer receptors exclusively activated by designer drugs (DREADD) system, Gq-protein-coupled receptor hM3D and its ligand clozapine-N-oxide (CNO), to activate the ACx-projecting cholinergic neurons (**Supplementary Fig. 4a, b and Supplementary Fig. 5)**. We expressed hM3D in cholinergic neurons by injecting AAV2/8-hSyn-DIO-hM3D(Gq)-mCherry into SI of ChAT-cre × YFP-H double transgenic mice, and injected CNO intraperitoneally to stimulate cholinergic neurons on imaging days 2 (as S1) and 3 (as S2). We found that the chemogenetic activation of cholinergic neurons could also increase spine formation after S1 but not S2 (**Supplementary Fig. 4c, d)**. These results further confirmed that cholinergic release in ACx could rapidly increase the formation of apical dendritic spines of L5 neurons.

Nicotinic AchRs, but not muscarinic AchRs, are involved in cholinergic

stimulation-induced spine formation

There are two major types of Ach receptors: nAchRs, an ionotropic receptor, and mAchRs, a metabolic receptor coupled with G-protein. Previous work has shown that both receptors are expressed in mouse cortical neurons[11]. To examine which type of AchR plays a key role in the cholinergic stimulation-induced spine formation, we selectively blocked nAchRs or mAchRs during optogenetic stimulation of cholinergic neurons by applying MEC, a nAchRs antagonist (*MEC & Opto*), or Scopolamine hydrobromide, a mAchRs antagonist (*Scopolamine & Opto*), respectively. For each mouse, 6 imaging sessions were performed (**Fig. 2a, b, c**). We found that blocking nAchRs effectively abolished the cholinergic stimulation-induced increase in spine formation, whereas blocking mAchRs does not have any significant effect (**Fig. 2d**). In addition, application of the two antagonists without optogenetic stimulation does not affect spine turnover (**Supplementary Fig. 6**). These results indicated that nAchRs, but not mAchRs, participated in triggering new spine formation in ACx.

Ach acts through GABAergic connections in triggering fast spine formation

Nicotinic AchRs are expressed both on the apical dendrites of cortical PNs and GABAergic interneurons. To determine whether Ach acts directly on PNs or via local inhibitory connections, we used bicuculline, the antagonist of γ-Aminobutyric acid type A receptors ($GABA_A$Rs), to block GABAergic synapses during the optogenetic stimulation (**Fig. 3a, b, c**). We found intraperitoneal bicuculline injection eliminated the cholinergic stimulation-induced increase in spine formation (**Fig. 3d**), suggesting that the local GABAergic transmission is necessary in the Ach-associated spine formation.

Cholinergic stimulation can also increase spine formation in PPC

Cholinergic neurons in the basal forebrain send projections broadly to sensory as well as higher-order cortical regions, such as posterior parietal cortex (PPC) [2, 18]. To determine whether the cholinergic stimulation-induced increase in spine formation is a general phenomenon for cortical regions receiving Ach projection, we further examined spine dynamics in PPC following chemogenetic stimulation of cholinergic neurons in SI. To locate the source of cholinergic projections to PPC, we first injected CTB-488 into PPC to retrogradely trace PPC-projection neurons (**Fig. 4a, b**). We then used immunostaining of ChAT to label cholinergic neurons. We identified PPC-projecting cholinergic neurons throughout the rostral-caudal axis of the basal forebrain, and found that they were dispersed over the whole basal forebrain (**Fig. 4c**). We then injected a Cre-dependent AAV- FLEX-EGFP into the basal forebrain of Chat-Cre transgenic mice. We observed GFP-labeled axon terminals in all layers of PPC (**Supplementary Fig. 1a, c**).

Similarly, we used the DREADD system to selectively activate the PPC-projecting cholinergic neurons (**Fig. 4d, e f**). We found that the chemogenetic activation of cholinergic neurons could also significantly increase spine formation after the first stimulation session (**Fig. 4g**). Together, these results suggested that the increased spine

formation on apical dendrites of L5 pyramidal neurons triggered by cholinergic neuron activation represented a general rule for spine plasticity.

The spatial distribution of newly formed spines along dendrites

The spatial distribution of spines along dendrites is a critical aspect of synaptic organization which plays an important role in regulating dendritic integration. To understand if cholinergic stimulation-triggered newly formed spines follow the same distribution pattern as the spontaneous new spines, we measured the distance between a new spine (n) and its nearest existing spine (s) ($D_{n–s}$) (**Fig. 5a**), and the distance between a new spine's two neighboring spines (D_{n-f}) (**Fig. 5f**) in NS and S1 groups. We found similar distribution patterns of $D_{n–s}$ (**Fig. 5b, c, d, e**) and D_{n-f} (**Fig. 5g, h, i, j**) in all groups. We also calculated the $D_{n–s}$ and D_{n-f} of newly formed spines that persisted over 1 day, and found no difference between different groups (**Supplementary Fig. 7**). Thus, cholinergic stimulation-induced new spines follow the same spatial rules as new spines formed spontaneously in physiological conditions.

Discussion

Synaptic plasticity is widely accepted as the cellular basis of learning and memory [19-21]. Formation or elimination of dendritic spines, the postsynaptic component of synapses, can represent the formation or elimination of synaptic connections [17, 22-24]. It is not clear how cholinergic system could affect the structural plasticity of synapses in cortical pyramidal neurons *in vivo*. In this study, using *in vivo* two-photon microscopy, we found that cholinergic activation could trigger increased spine formation on apical dendrites of layer 5 pyramidal neurons in ACx within 4 hours. These new spines were susceptible to elimination, as were the new spines formed without Ach stimulation (**Supplementary Fig. 3**). We measured the distance between new formed spines and existing spines, and found that cholinergic stimulation-induced new spines follow the same spatial rule as new spines formed in physiological conditions.

Formation of spines requires expression and transportation of various proteins, kinases and phosphatases such as Calmodulin, Calcineurin, Cofilin, Arp2/3, Actin and etc [25]. We found that a second stimulation session on the day after the first stimulation session could not induce increased spine formation, possibly due to limited cellular resource. Thus, it is likely that cholinergic stimulation triggers transportation and insertion of local postsynaptic proteins to form new spines, rather than translation of synaptic proteins. How acetylcholine recruits these proteins to form new spines remains to be elucidated.

Consistent with previous studies, we found that nAchRs play an important role in synaptic structural plasticity [13-15, 26, 27]. But we also found that the increase in spine formation depends on local GABAergic connections, rather than autonomous

nAchR activation (as was demonstrated in [12], activation of beta2-nAchR increases spine density via autonomous mechanisms). The differences could be explained by different brain regions (hippocampus vs. cortex) and different stimulation protocols: we used optogenetic/chemogenetic stimulation lasting only 4 hours, rather than nicotinic activation lasting 11 days.

An important cortical disinhibitory microcircuit consists of VIP-expressing interneurons, which inhibit SOM-or PV-expressing interneurons that subsequently disinhibit the apical dendrites or perisomatic regions of pyramidal neurons, respectively [1, 28, 29]. To examine if the increased spine formation induced by activating the cholinergic neurons were directly related to nAchRs on apical dendrites or indirectly via local GABAergic connections, we applied bicuculline, the antagonist of $GABA_A$Rs, during the optogenetic stimulations. We found that bicuculline application eliminated the cholinergic stimulation-induced increase in spine formation. Thus, local inhibitory circuit is necessary for Ach induced spine formation. Previous studies showed that SOM-expressing interneurons mainly inhibit the distal dendrites of L2/3 pyramidal neurons in motor cortex, and PV-expressing interneurons mainly inhibit the perisomatic compartment of pyramidal neurons [30]. Which subtypes of GABAergic neurons are involved in this process needs to be further studied.

Cholinergic neurons in the basal forebrain project extensively to mouse neocortex. We observed similar increase in spine formation in ACx and PPC, suggesting that the increased spine formation on apical dendrites of L5 pyramidal neurons triggered by cholinergic neuron activation might be a general rule of spine plasticity for both sensory and association cortex.

Materials and methods

Animals

All procedures were permitted by the Animal Care and Ethics Committee at the School of Science and Technology, ShanghaiTech University. Chat-Cre, Ai32, and YFP-H (Thy1-YFP) transgenic mice were obtained from Jackson Laboratories. The Chat-Cre mouse line was crossed with the YFP-H line to acquire the Chat-Cre x Thy1-YFP mouse line. Then the Chat-Cre x Thy1-YFP mouse line was crossed with the Ai32 mouse line to get the Chat-Cre x Ai32 x Thy1-YFP-H mouse line. All mice were housed and bred in a 12/12h light-dark cycle (8 a.m.-8 p.m. light) in the animal facility of the ShanghaiTech with ad libitum water and food. Mice used for viral delivery were 5-6 weeks old. Mice used for imaging experiments were 9-14 weeks old. Each mouse was individually housed after fiberoptic implantation.

Surgery and virus injection

AAV2/9-CAG-FLEX-EGFP, AAV2/8-hSyn-FLEX-chrimsonR-tdTomamto, AAV2/8-hSyn-DIO-hM3D(Gq)-mCherry were purchased from OBiO Technology Co., Shanghai, China.

Mice were anesthetized with isoflurane (1%-1.5%) and positioned in a stereotaxic apparatus (Reward Co., Shenzhen, China). Body temperature was maintained at 37°C using a mini-blanket and heating pad during all surgery and imaging process. Viruses were injected using a glass electrode with a tip diameter of 20–25 μm via a small skull opening (<0.4 mm^2) with a micro-injector (Nanoject3, Drummond Scientific Co., Broomall, United States). Viruses were diluted to 1 x 10^{13} or 6 x 10^{12} vg/ml, 50-150 nl/injection site (1nl/s). The stereotaxic coordinates were as follows: ACx (AP: -2.45 mm, ML: -4.4 mm, DV: -1.1 mm); SI (1. AP: -1.25 mm, ML: -2.36 mm, DV: -3.8 mm; 2. AP: -1.45 mm, ML: -2.52 mm, DV: -3.75 mm); PPC (1. AP: -1.95 mm, ML: -1.55 mm, DV: -0.3 mm, -0.55 mm; 2. AP: -2.3mm, ML: -2.55 mm, DV: -0.6 mm; 3. AP: -2.45 mm, ML: -2.75 mm, DV: -0.5 mm); basal forebrain (1. AP: +0.6 mm, ML: -0.52 mm, DV: -4.9 mm; 2. AP: +0.2 mm, ML: -1.0 mm, DV: -5.1 mm; 3. AP: -0.5 mm, ML: -1.7 mm, DV: -4.8mm, -3.75 mm; 4. AP: -1.2 mm, ML: -1.7 mm, DV: -4.8mm, -4.1 mm; 5. AP: -1.4 mm, ML: -2.4 mm, DV: -3.5 mm).

For optogenetic stimulation of SI, the optic fiber (0.37 N.A., 200 μm diameter, 4.5mm length, Inper Co., Hangzhou, China) was implanted ~ 200 μm above the coordinates for viral injection, and the stereotaxic coordinates were as follows: AP: -1.4 mm, ML: -2.45 mm, DV: -3.5 mm.

For chronic cranial imaging window implantation, mice were anesthetized with isoflurane (1%-5%) and positioned in a stereotaxic apparatus (Reward Co.). The skin, subcutaneous tissue, and muscle above the ACx were removed to expose the skull with a scalpel. A 1.5 x 1.8 mm^2 skull over the ACx was replaced by a 1.5 x1.8 mm^2 inner layer and a 2 x 3 mm^2 outer layer cover-glass window. For the cranial window of PPC, a 3 mm diameter skull over the PPC was replaced by a 3 mm inner diameter and 3.5 mm outside diameter circular cover-glass window; the center stereotaxic coordinates were as follows: AP: -2.1 mm, ML: -2.0 mm. The double-layer cover glass was glued via UV-curing glue. A thin layer of super glue was applied to the edges of the cover glass to seal the cranial window. A custom-made head-post was attached to the skull by dental cement for fixed the mouse head during two-photon imaging. Mice that have completed the cranial window have recovered for at least two weeks before performing imaging experiments.

After the last imaging session, imaging positions were verified by injecting DiI (10-20 nl) into the cortex according to the vascular pattern of the imaging field. Then the mice were perfused immediately using 0.01M phosphate-buffered saline (PBS) and 4% paraformaldehyde (PFA), sliced (~100 um) by vibratome (Leica VT1200S, Wetzlar, Germany) after post-fixed overnight to confirm the imaging position and virus expression.

Retrograde labeling of ACx or PPC projection cholinergic neurons

For retrograde labeling ACx or PPC projection neurons, mice were anesthetized with

isoflurane (1%-5%) and positioned in a stereotaxic apparatus (Reward Co.). 500 nl CTB-488 was injected into ACx or PPC using a micro-injector (Nanoject3, Drummond Scientific Co.). After allowing 10 days for retrograde transport, mice were perfused using 0.01M PBS and 4% PFA, sliced (~50 um) by vibratome (Leica VT1200S, Wetzlar, Germany) after post-fixed overnight. The injection site was confirmed (Figure 1a, Figure 4a). All brain slices containing basal forebrain were dealt with CHAT immunostaining.

Immunofluorescence

The primary antibodies were as follows: goat-anti-CHAT (AB144P, Millipore, Temecula, CA, United States, 1:1000), guinea pig-anti-cFos (226308, Synaptic system, Germany, 1:800). The secondary antibodies were as follows: AlexaFluor 647-conjugated donkey-anti-goat (A-21447, ThermoFisher Scientific, Waltham, MA, United States, 1:1000), AlexaFluor 647-conjugated donkey-anti-guinea pig (K0040D-AF647, Solarbio Life Sciences, Beijing, China, 1:1000). CNO or Saline treatment mice were perfused ~4h after the first administration using 0.01M PBS and 4% PFA, sliced (~40 um) by vibratome (Leica VT1200S) after post-fixed overnight. Brain slices were permeabilized with 0.4% Triton X-100 for 30 minutes and blocked with 5% bovine serum albumin (BSA)/PBS for 1 h, then incubated with the primary antibody in 0.02% Triton X-100 and 1% BSA/PBS for 48h at 4°C, then washed with PBS 3 x 10 minutes and incubated with DPAI (1:2500) and the secondary antibody in 0.02% Triton X-100 and 1% BSA /PBS for 2h at room temperature, then washed with PBS 3 x 10 minutes. The brain slices were imaged on a confocal microscope (Nikon CSU-W1).

Tone and optogenetic manipulation

For Tone only stimulation, 6 kHz, 70-75 dB SPL, 2s duration, 5-15 s inter-trial interval (ITI) pure tone controlled by a Bpod state machine (Sanworks Co., Rochester, NY, United States) and open-source Bpod software (Sanworks Co.) were played via a speaker placed on the right side of mice, 1200 trials, ~ 4h.

For paired tone and optogenetic stimulation, the laser stimulus was delivered 1 s after the sound onset. The laser was connected to the implanted optic fiber before each imaging session. For ChR2-mediated cholinergic activation, we used a 473 nm laser (LSR473NL-50-FC, lasever etlong Co., NingBo, China) at a power of 5–10 mW/mm^2 at the fiber tip, for ChrimsonR-mediated cholinergic activation, we used a 589 nm laser (LSR589H-50-FC, lasever etlong Co.) at a power of 5-10 mW/mm^2 at the fiber tip. The laser transmission frequency is controlled by PulsePal (Open Ephys) with 20Hz, 1s duration, and 20 pulses; each pulse has a 5 ms duration and 45 ms interval, 1200 trials, ~4h. The protocol of optogenetic only stimulation was the same with paired tone and optogenetic stimulation but without tone playing.

Drug administration

Clozapine-N-oxide (CNO) (5mg/kg i.p.), saline, Scopolamine hydrobromide (1mg/kg i.p., MedChemExpress, Shanghai, China), Mecamylamine hydrochloride (MEC, MedChemExpres) (1mg/kg i.p.), Bicuculline (5mg/kg i.p., MedChemExpress) or

vehicle (10% DMSO & 90% corn oil) were administered in 4 divided doses at intervals of 1 h respectively during the first and second stimulation sessions (the first administration was 15 min before stimulation).

Two-photon structural imaging

Mice were habituated to the environment of two-photon imaging the day before the first imaging session. Mice were anesthetized with isoflurane (1%-2%) and head-fixed using the custom-made head-post. Image stacks were obtained with a step of 0.7 um from the cortical surface to 100-150 um deep using a two-photon microscope (Bergamo II, Thorlabs, Newton, NJ, United States) equipped with a water-immersion 25X 1.05 NA objective (Olympus, Kyoto, Japan) and a Mai Tai Deep See Ti:sapphire laser (Spectra-Physics) at 920 nm. The output optical power <40 mW to avoid phototoxicity. A digital zoom of 6 was used.

Imaging data analysis

We used an open-source image processing toolbox ORCA (Online Real-time activity and offline Cross-session Analysis) [31] to remove the motion artifacts caused by the respiration and heartbeat of mice. After the image registration, all images were analyzed manually on the three-dimensional stacks using ImageJ and blind to experimental conditions. The same dendritic fragments that were recognizable in all 6 imaging sessions were used for analysis. For spine identification, we adopted criteria from ref. [32]. In short, the length/neck diameter ratio >3 and head/ neck diameter ratio <1.2 of dendritic protrusions (length more than 1/3 diameter of dendritic shaft) were defined as filopodia and other protrusions were classified as spines. Spine formation or elimination was based on the comparison of adjacent imaging sessions. The total number of spines analyzed for each mouse was more than 180. All distance measurements were done by the semi-automatic ImageJ plugin, Simple Neurite Tracer, in three-dimensional stacks.

Statistics

All statistical analyses were performed using GraphPad Prism. Two-sided paired Student's t-tests were used for paired comparisons in Figure 1g, Figure 2d, Figure 3d, Figure 4g and Supplementary Figure 4d, Supplementary Figure 6d. Two-sided unpaired Student's t-tests were used for unpaired comparisons in Supplementary Figure 5c. Mann-Whitney U-test was used for comparisons in spine distance data in Figure 5 and Supplementary Figure 3, 7.

Acknowledgements

We thank Drs. Yu Xin and Jun-Qian Qi for suggestions on chronic window surgery; the Molecular Imaging Core Facility at ShanghaiTech University for technical support in confocal imaging; and the animal facility of ShanghaiTech for their excellent care of mice.

Author contributions

X.Z. and Y.Y. conceived the project. X.Z., Y.Z. and L.Y. performed the experiments and

analyzed the data. X.Z. and Y.Y. wrote the manuscript.

Competing interests

The authors declare no competing financial interests.

References

1. Zaborszky, L., et al., *Specific Basal Forebrain-Cortical Cholinergic Circuits Coordinate Cognitive Operations.* J Neurosci, 2018. **38**(44): p. 9446-9458.
2. Mesulam, M.M., et al., *Central cholinergic pathways in the rat: an overview based on an alternative nomenclature (Ch1-Ch6).* Neuroscience, 1983. **10**(4): p. 1185-201.
3. Butt, A.E., et al., *Association learning-dependent increases in acetylcholine release in the rat auditory cortex during auditory classical conditioning.* Neurobiol Learn Mem, 2009. **92**(3): p. 400-9.
4. Leach, N.D., et al., *Cortical cholinergic input is required for normal auditory perception and experience-dependent plasticity in adult ferrets.* J Neurosci, 2013. **33**(15): p. 6659-71.
5. Kilgard, M.P. and M.M. Merzenich, *Cortical map reorganization enabled by nucleus basalis activity.* Science, 1998. **279**(5357): p. 1714-8.
6. Froemke, R.C., *Plasticity of cortical excitatory-inhibitory balance.* Annu Rev Neurosci, 2015. **38**: p. 195-219.
7. Weinberger, N.M., *Associative representational plasticity in the auditory cortex: a synthesis of two disciplines.* Learn Mem, 2007. **14**(1-2): p. 1-16.
8. McLin, D.E., 3rd, A.A. Miasnikov, and N.M. Weinberger, *Induction of behavioral associative memory by stimulation of the nucleus basalis.* Proc Natl Acad Sci U S A, 2002. **99**(6): p. 4002-7.
9. Froemke, R.C., et al., *Long-term modification of cortical synapses improves sensory perception.* Nat Neurosci, 2013. **16**(1): p. 79-88.
10. Froemke, R.C., M.M. Merzenich, and C.E. Schreiner, *A synaptic memory trace for cortical receptive field plasticity.* Nature, 2007. **450**(7168): p. 425-9.
11. Colangelo, C., et al., *Cellular, Synaptic and Network Effects of Acetylcholine in the Neocortex.* Front Neural Circuits, 2019. **13**: p. 24.
12. Oda, A., et al., *Nicotine induces dendritic spine remodeling in cultured hippocampal neurons.* J Neurochem, 2014. **128**(2): p. 246-55.
13. Lozada, A.F., et al., *Induction of dendritic spines by beta2-containing nicotinic receptors.* J Neurosci, 2012. **32**(24): p. 8391-400.
14. Lozada, A.F., et al., *Glutamatergic synapse formation is promoted by alpha7-containing nicotinic acetylcholine receptors.* J Neurosci, 2012. **32**(22): p. 7651-61.
15. Schatzle, P., et al., *Rapid and reversible formation of spine head filopodia in response to muscarinic receptor activation in CA1 pyramidal cells.* J Physiol, 2011. **589**(17): p. 4353-64.
16. Guo, L., et al., *Dynamic rewiring of neural circuits in the motor cortex in mouse models of Parkinson's disease.* Nat Neurosci, 2015. **18**(9): p. 1299-1309.
17. Yang, G., F. Pan, and W.B. Gan, *Stably maintained dendritic spines are associated with lifelong memories.* Nature, 2009. **462**(7275): p. 920-4.

18. Bucci, D.J., M. Conley, and M. Gallagher, *Thalamic and basal forebrain cholinergic connections of the rat posterior parietal cortex.* Neuroreport, 1999. **10**(5): p. 941-5.
19. Kandel, E.R., *The biology of memory: a forty-year perspective.* J Neurosci, 2009. **29**(41): p. 12748-56.
20. Holtmaat, A. and K. Svoboda, *Experience-dependent structural synaptic plasticity in the mammalian brain.* Nat Rev Neurosci, 2009. **10**(9): p. 647-58.
21. Holtmaat, A. and P. Caroni, *Functional and structural underpinnings of neuronal assembly formation in learning.* Nat Neurosci, 2016. **19**(12): p. 1553-1562.
22. Xu, T., et al., *Rapid formation and selective stabilization of synapses for enduring motor memories.* Nature, 2009. **462**(7275): p. 915-9.
23. Peters, A.J., S.X. Chen, and T. Komiyama, *Emergence of reproducible spatiotemporal activity during motor learning.* Nature, 2014. **510**(7504): p. 263-7.
24. Qiao, Q., et al., *Motor learning-induced new dendritic spines are preferentially involved in the learned task than existing spines.* Cell Rep, 2022. **40**(7): p. 111229.
25. Valles, A.S. and F.J. Barrantes, *Dendritic spine membrane proteome and its alterations in autistic spectrum disorder.* Adv Protein Chem Struct Biol, 2022. **128**: p. 435-474.
26. Morley, B.J. and R.F. Mervis, *Dendritic spine alterations in the hippocampus and parietal cortex of alpha7 nicotinic acetylcholine receptor knockout mice.* Neuroscience, 2013. **233**: p. 54-63.
27. Ballesteros-Yanez, I., et al., *Alterations of cortical pyramidal neurons in mice lacking high-affinity nicotinic receptors.* Proc Natl Acad Sci U S A, 2010. **107**(25): p. 11567-72.
28. Askew, C.E., et al., *Nicotine excites VIP interneurons to disinhibit pyramidal neurons in auditory cortex.* Synapse, 2019. **73**(9): p. e22116.
29. Kamigaki, T., *Dissecting executive control circuits with neuron types.* Neurosci Res, 2019. **141**: p. 13-22.
30. Chen, S.X., et al., *Subtype-specific plasticity of inhibitory circuits in motor cortex during motor learning.* Nat Neurosci, 2015. **18**(8): p. 1109-15.
31. Sheng, W., et al., *Real-Time Image Processing Toolbox for All-Optical Closed-Loop Control of Neuronal Activities.* Front Cell Neurosci, 2022. **16**: p. 917713.
32. Holtmaat, A., et al., *Long-term, high-resolution imaging in the mouse neocortex through a chronic cranial window.* Nat Protoc, 2009. **4**(8): p. 1128-44.

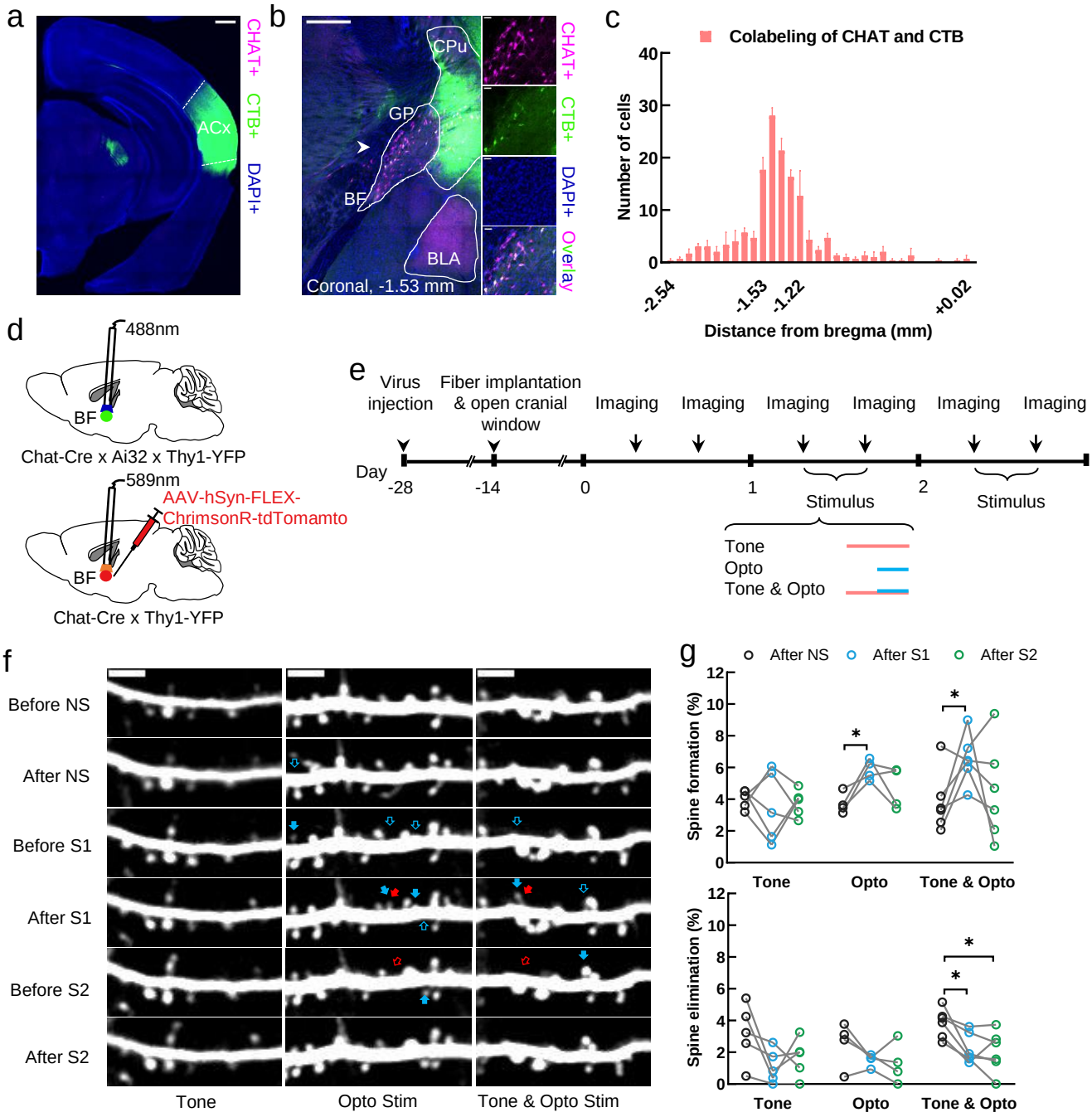

Figure 1. Optogenetic activation of cholinergic neurons increases spine formation on apical dendrites of L5 PNs in the auditory cortex. (a) Image showing CTB injection site in ACx. Scale bar, 500um. (b) Image showing cholinergic (ChAT+) neurons retrogradely labeled by CTB injection in ACx. CPu, caudate putamen; BLA, basolateral amygdala; BF, basal forebrain. Scale bar, 500um (left), 50um (right). (c) Distribution of labeled ACx-projecting ChAT+ neurons in the basal forebrain along the rostral-caudal axis. n=3, Error bars, s.e.m. (d, e) Experimental timeline for virus injection, chronic window implantation, and two-photon imaging. (f) Example images obtained by repeated imaging of the same apical dendrites of ACx L5 PNs in 3 experimental conditions: Tone, optogenetic stimulation (Opto), and paired tone and optogenetic stimulation (Tone & Opto). Cyan arrows, newly formed spines. Red arrows, eliminated spines. Scale bar, 4 µm. NS, no manipulation; S1, stimulation on day 1; S2, stimulation on day 2. (g) Percentages of spine formation and elimination of apical dendrites of L5 PNs in Tone, Opto, and Tone & Opto groups after no manipulation (NS), first stimulation session (S1) and second stimulation session (S2) (Tone, n=5; Opto, n=4, Tone & Opto, n=6. Paired t-test. *P<0.05).

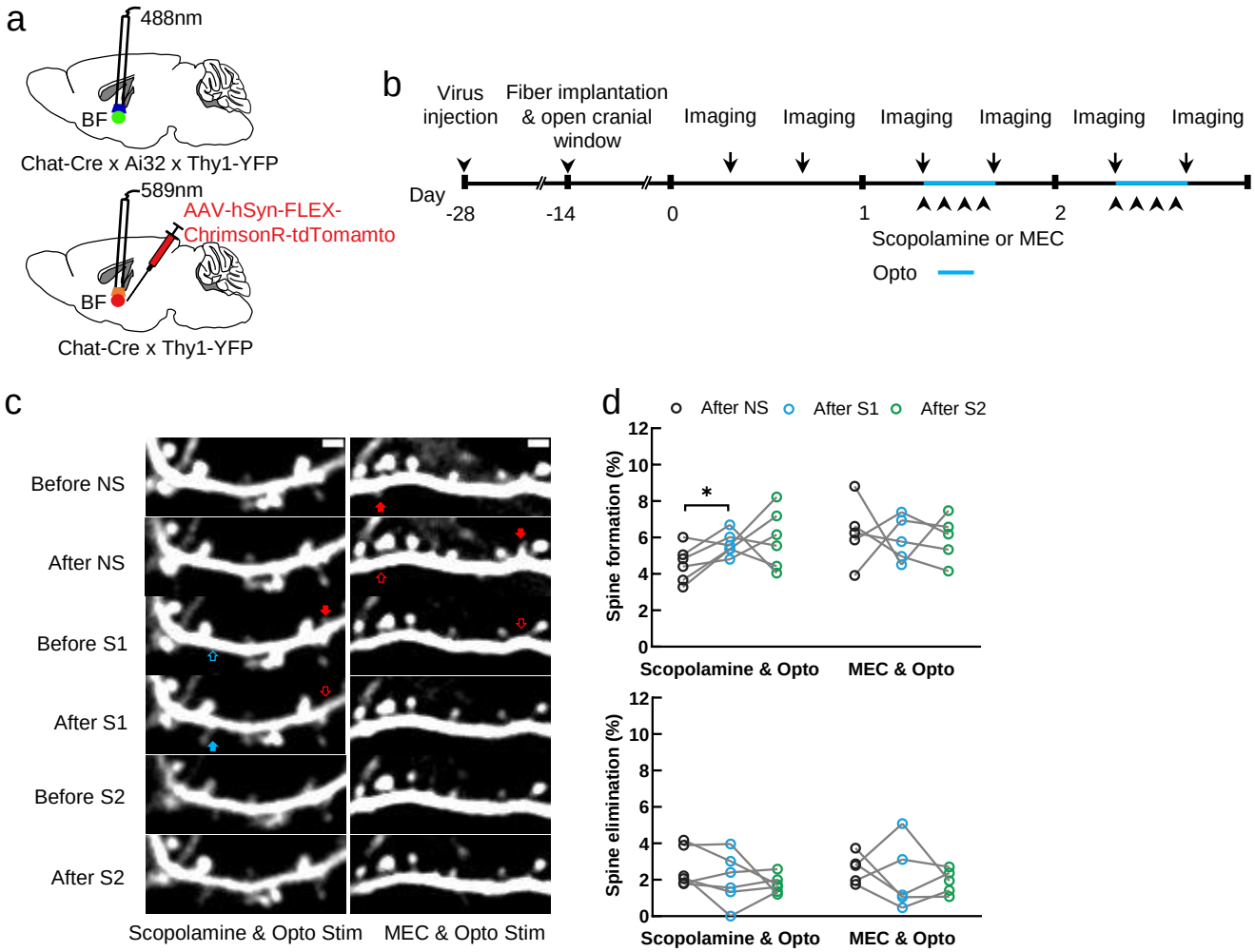

Figure 2. Blocking nAchRs affects optogenetic stimulation-induced ACx spine formation. (a, b) Experimental timeline. (c) Example images obtained by repeated imaging of the same apical dendrites of ACx L5 PNs in 2 experimental conditions: Scopolamine & Opto Stim and MEC & Opto Stim. Cyan arrows, newly formed spines. Red arrows, eliminated spines. Scale bar, 2 µm. NS, no manipulation; S1, stimulation on day 1; S2, stimulation on day 2. (d) Percentages of spine formation and elimination of apical dendrites of L5 PNs in Scopolamine & Opto and MEC & Opto groups after no manipulation (NS), first stimulation session (S1) and second stimulation session (S2) (Scopolamine & Opto, n=6; MEC & Opto, n=5. Paired t-test. *P<0.05).

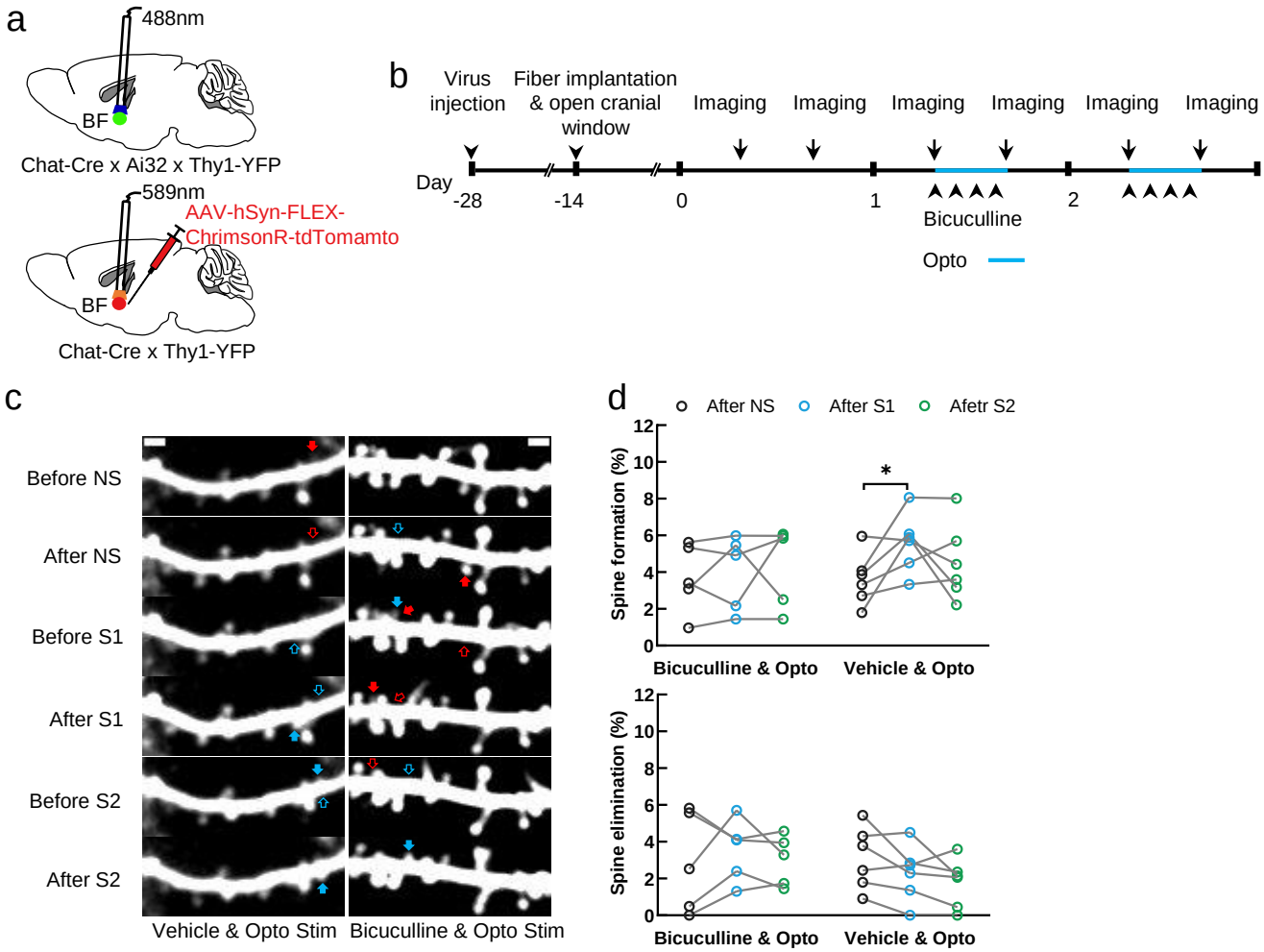

Figure 3. Blocking GABAA receptors affects optogenetic stimulation-induced ACx spine formation. (a, b) Experimental timeline. (c) Example images obtained by repeated imaging of the same apical dendrites of ACx L5 PNs in 2 experimental conditions: Bicuculline & Opto Stim and Vehicle & Opto Stim. Cyan and red arrows, newly formed and eliminated spines. Scale bars, 2 µm. NS, no manipulation; S1, stimulus on day1; S2, stimulus on day2. (d) Percentages of spine formation and elimination of apical dendrites of L5 PNs in Bicuculline & Opto and Vehicle & Opto groups after NS, first stimulation session (S1) and second stimulation session (S2) (Bicuculline & Opto, n=5 Vehicle & Opto, n=6. Paired t-test. *P<0.05, **P<0.01).

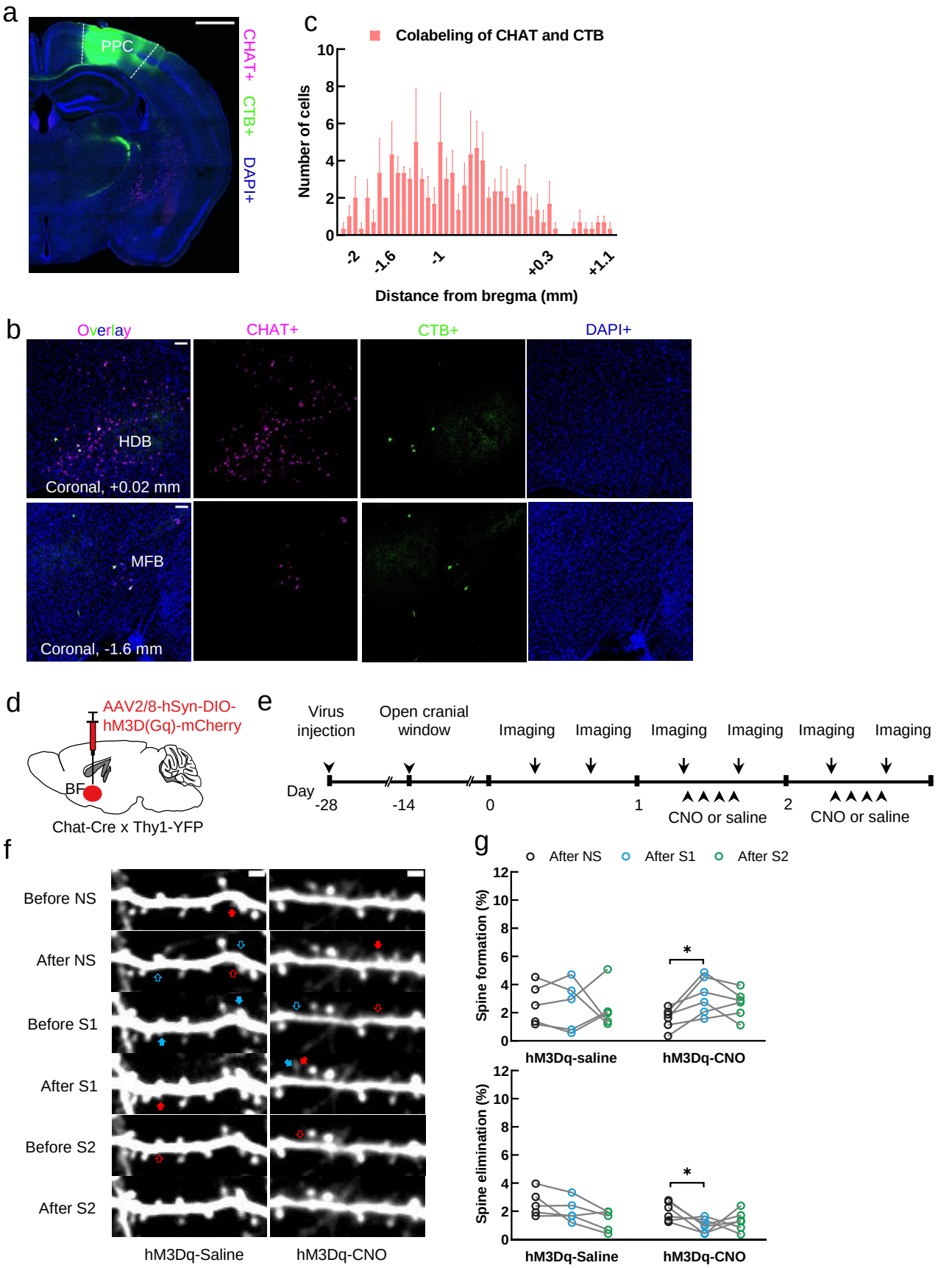

Figure 4. Chemogenetic activation of cholinergic neurons increases spine formation on apical dendrites of L5 PNs in PPC. (a) Image showing CTB injection site in PPC. Scale bar, 500um. (b) Image showing cholinergic (ChAT+) neurons retrogradely labeled by CTB in PPC. HDB, nucleus of the horizontal limb of the diagonal band; MFB, medial forebrain bundle. Scale bar, 50um. (c) Distribution of labeled PPC-projecting ChAT+ neurons in the basal forebrain along the rostral-caudal axis. n=3, Error bars, s.e.m. (d, e) Experimental timeline for virus injection, chronic window implantation, and two-photon imaging. (f) Example images obtained by repeated imaging of the same apical dendrites of PPC L5 PNs neurons in 2 experimental conditions: hM3Dq-Saline and hM3Dq-CNO. Cyan and red arrows, newly formed and eliminated spines. Scale bars, 2 µm. NS, no manipulation; S1, stimulus on day1; S2, stimulus on day2. (g) Percentages of spine formation and elimination of apical dendrites of L5 PNs in hM3Dq-Saline and hM3Dq-CNO groups after no manipulation (NS), after first stimulation session (S1) and second stimulation session (S2) (Saline, n=5; CNO, n=6. Paired t-test. *P<0.05, **P<0.01).

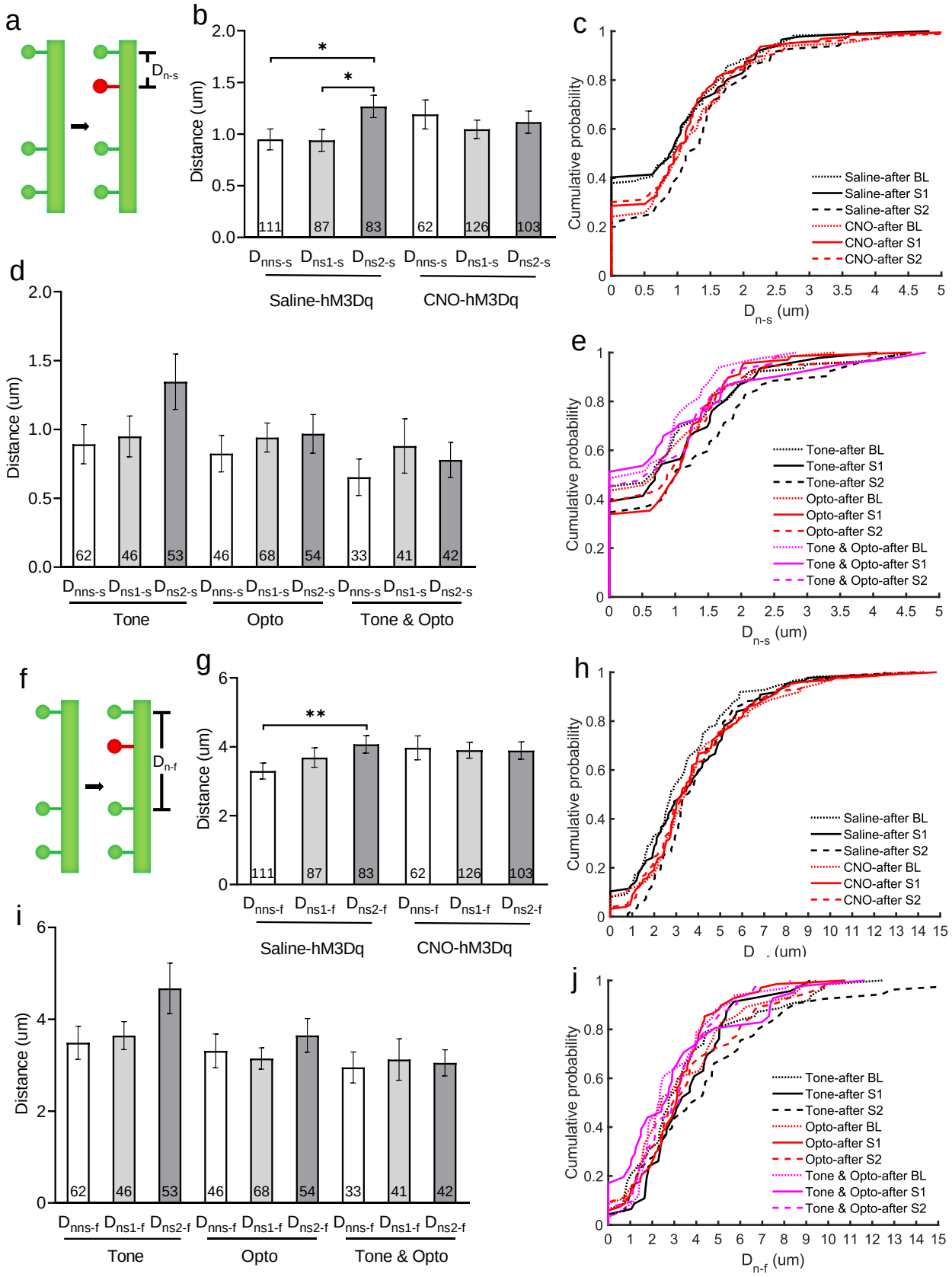

Figure 5. The spatial distribution of new spines along dendrites. (a) Schematic illustration of the measurement of D_{n-s}, the distance between a new spine (n) and its nearest existing spine (s). (b, d) D_{n-s} of mice in each treatment. D_{nns-s}, D_{n-s} of the newly formed spine after no manipulation; D_{ns1-s}, D_{n-s} of the newly formed spine after S1; D_{ns2-s}, D_{n-s} of the newly formed spine after S2. (c, e) Cumulative probability distribution of D_{n-s} in each treatment. (f) Schematic illustrating the measurement of D_{n-f}, the distance between a new spine's two neighboring spines. (g, i) D_{n-f} of mice in each treatment. D_{nns-f}, D_{n-f} of the newly formed spine after no manipulation; D_{ns1-f}, D_{n-f} of the newly formed spine after S1; D_{ns2-f}, D_{n-f} of the newly formed spine after S2. (h, j) Cumulative probability distribution of D_{n-f} in each treatment. The number of spines analyzed is indicated in each column. Mann-Whitney U-test, *P<0.05, **P<0.01. Error bars, s.e.m.

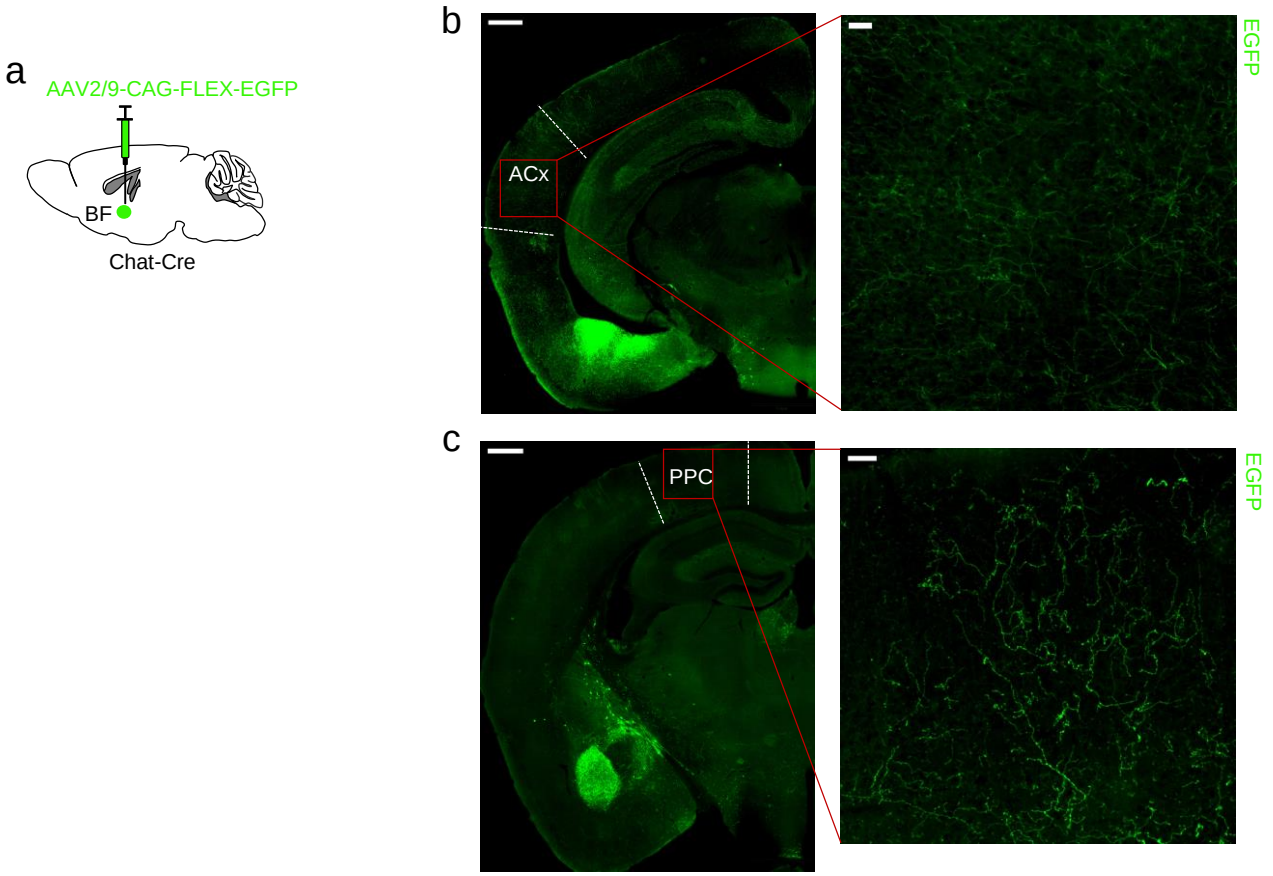

Supplementary Figure 1. The axonal terminals of cholinergic neurons in the ACx and PPC. (a) Scheme of virus tracing of cholinergic neurons in ChAT-Cre mice. (b)The axonal terminals of cholinergic neurons are widely distributed in the ACx. Scale bar, 500um left, 50um right. (c) The axonal terminals of cholinergic neurons are widely distributed in the PPC. Scale bar, 500um left, 50um right.

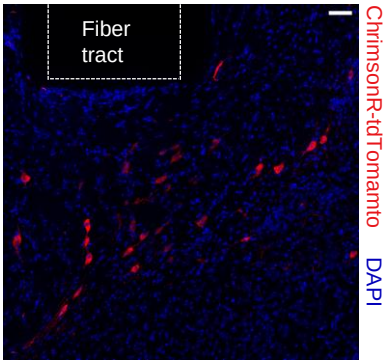

Supplementary Figure 2. Expression of ChrimsonR-tdTomato in BF cholinergic neurons. Scale bar, 50 µm.

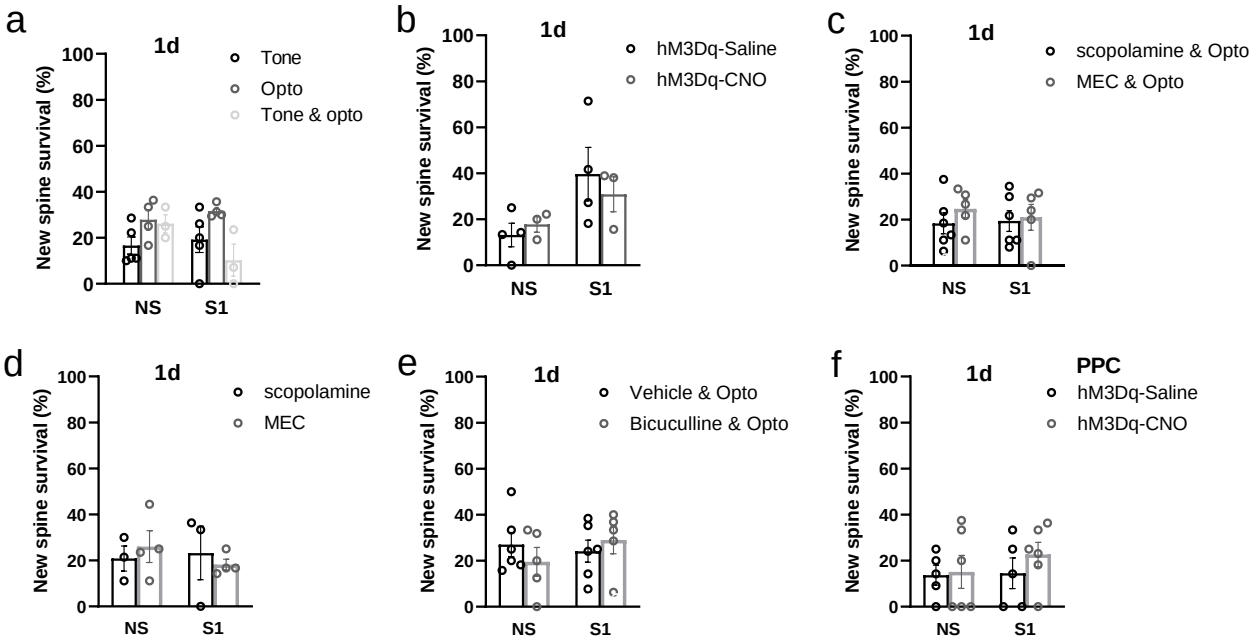

Supplementary Figure 3. The proportion of new spine survival after 1 d. (a) Tone, n=5; Opto, n=4; Tone & Opto, n=3. (b) Saline n=4; CNO n=3. (c) Scopolamine & Opto, n=6; MEC & Opto, n=5. (d) Scopolamine, n=3; MEC, n=4. (e) Bicuculline & Opto, n=5; Vehicle & Opto, n=6. (f) Saline, n=5; CNO, n=6. Error bars, s.e.m.

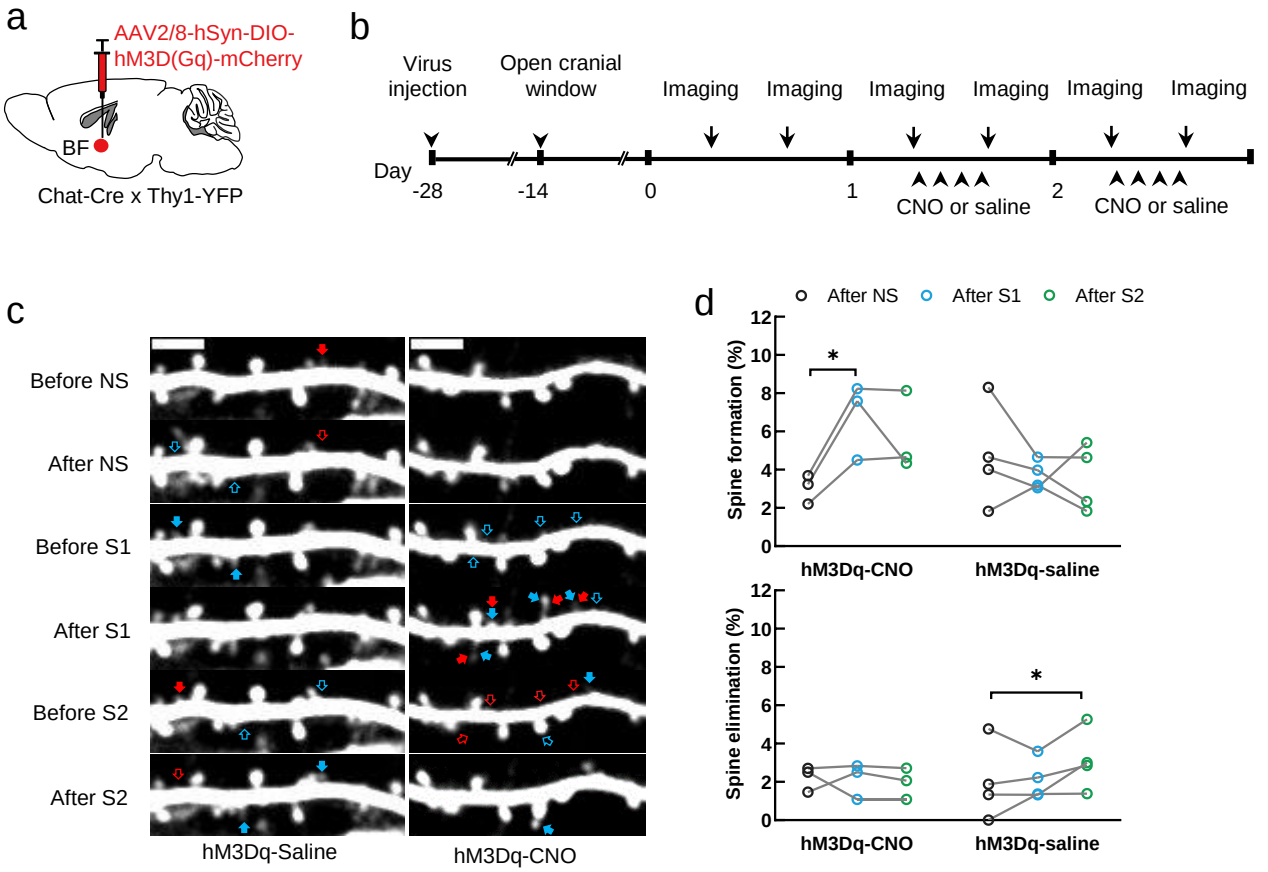

Supplementary Figure 4. Chemo-genetic activation of cholinergic neurons increases the formation of apical dendritic spines of L5 PNs in the auditory cortex. (a,b) Experimental timeline for virus injection, chronic window implantation, and two-photon imaging. (c) Example images obtained by repeated imaging of the same apical dendrites of ACx L5 PNs in 2 experimental conditions: hM3Dq-Saline and hM3Dq-CNO. Cyan arrows, newly formed spines. Red arrows, eliminated spines. Scale bars, 4 µm. NS, no manipulation; S1, stimulus on day1; S2, stimulus on day2. (d) Percentages of spine formation and elimination of apical dendrites of L5 PNs in hM3Dq-Saline and hM3Dq-CNO groups after no manipulation (NS), after first stimulation session (S1) and second stimulation session (S2) (hM3Dq-Saline, n=4; hM3Dq-CNO, n=3. Paired t-test. *P<0.05).

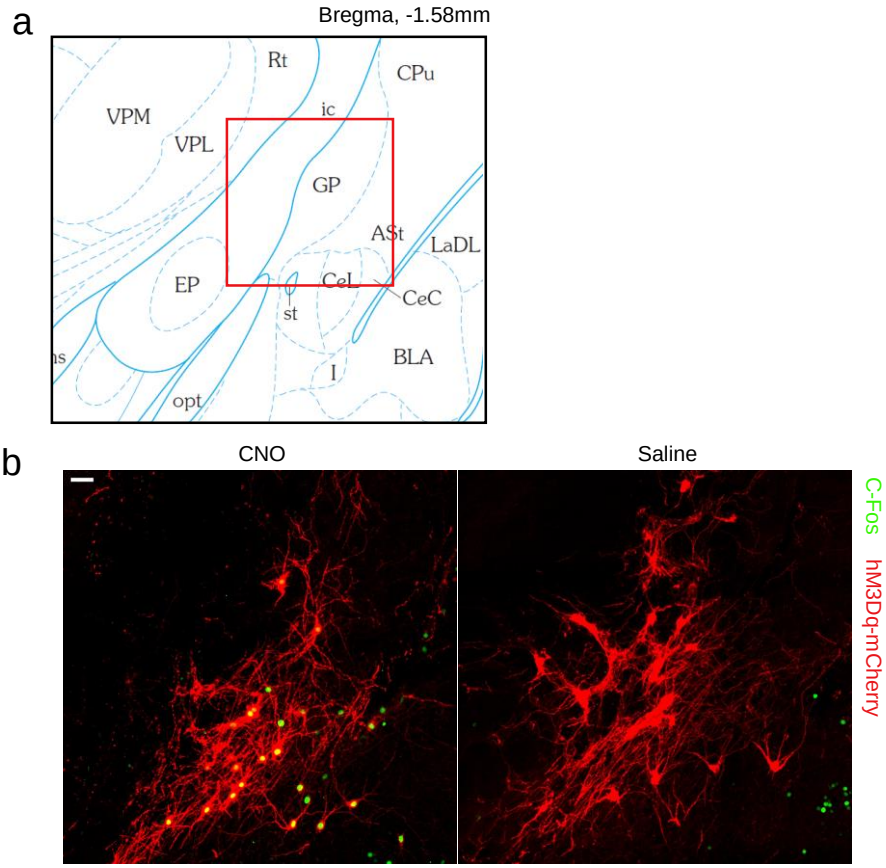

Supplementary Figure 5. Co-expression of c-Fos and hM3Dq in BF in DREADD. (a) Schematic illustrating the location of GP. The red box indicates the position of the images shown in b. (b) Representative images showing CNO selectivity activated DREADD virus-infected neurons. scale bar, 50 um. (c) Expressing of c-Fos+ of cholinergic neurons in mice receiving CNO or saline injection (Saline n=3; CNO n=3. unpaired t-tests, **** P<0.0001). Error bars, s.e.m.

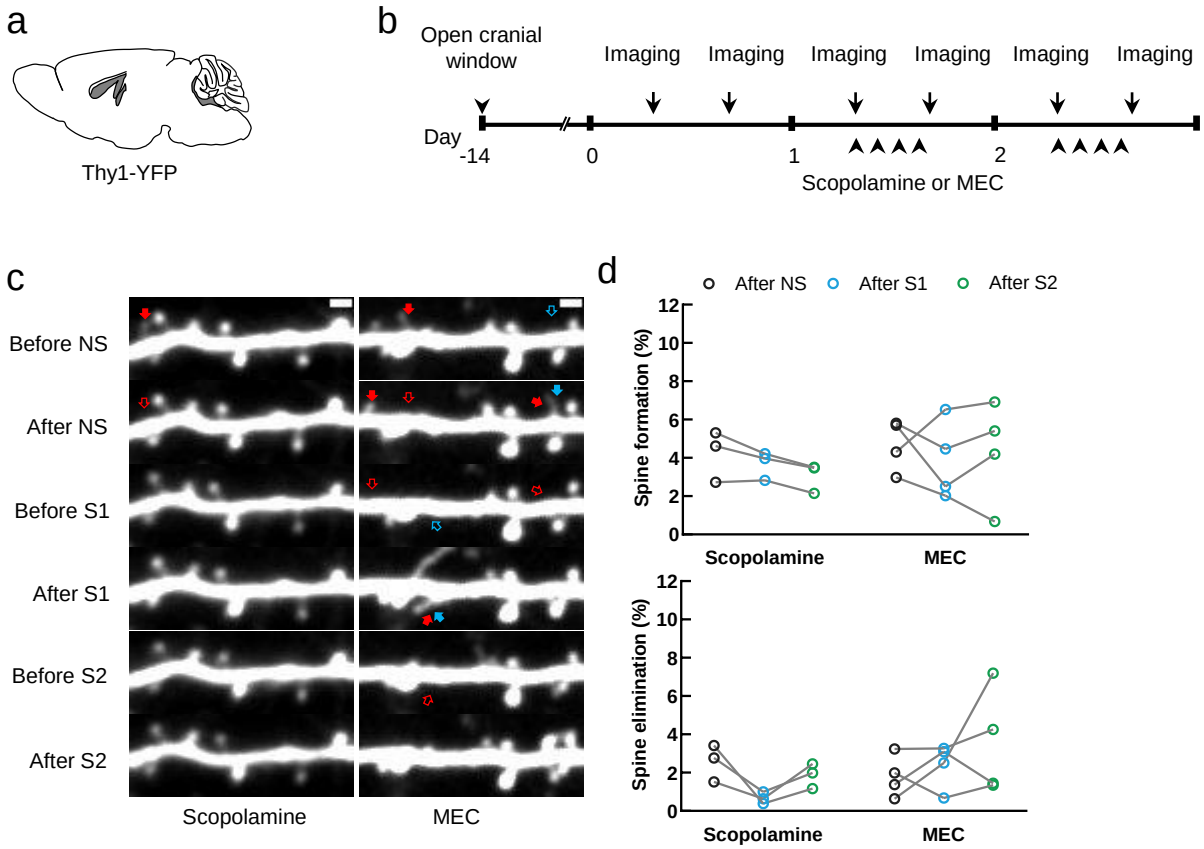

Supplementary Figure 6. Blocking AchRs has no effects on spontaneous spine dynamics of ACx. (a, b) Experimental timeline. (c) Example images obtained by repeated imaging of the same apical dendrites of ACx L5 PNs in 2 experimental conditions: Scopolamine Stim and MEC Stim. Cyan arrows, newly formed spines. Red arrows, eliminated spines. Scale bar, 2 µm. NS, no manipulation; S1, stimulation on day 1; S2, stimulation on day 2. (d) Percentages of spine formation and elimination of apical dendrites of L5 PNs in Scopolamine and MEC groups after no manipulation (NS), first stimulation session (S1) and second stimulation session (S2) (Scopolamine, n=3; MEC, n=4).

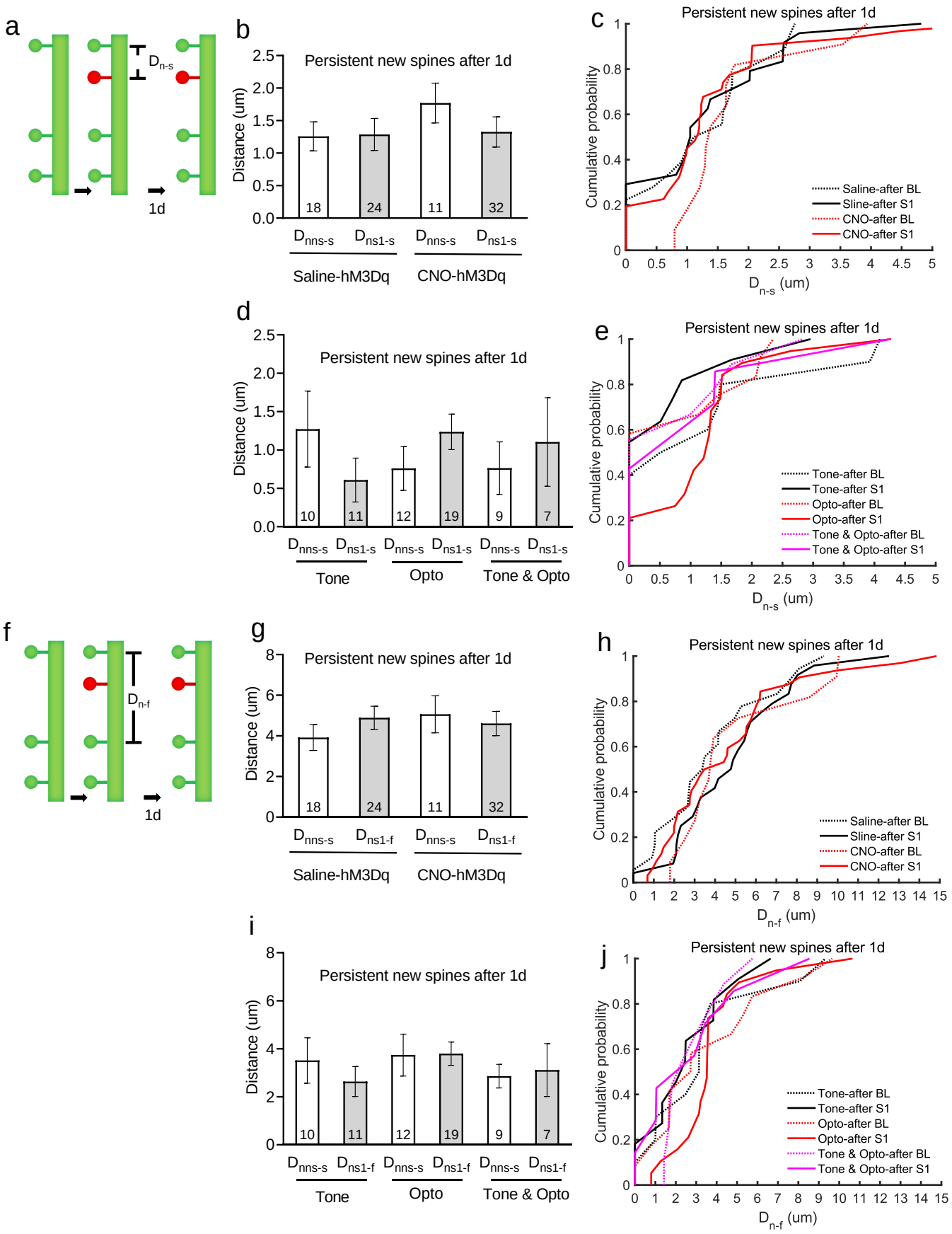

Supplementary Figure 7. The spatial distribution of persistent new spines along dendrites. (a, f) Schematic illustration of the measurement of D_{n-s} or D_{n-f} of persistent new spines after 1d. (b, d, g, i) D_{n-s} or D_{n-f} in each treatment. (c, e, h, j) Cumulative probability distribution of D_{n-s} or D_{n-f} in each treatment. Error bars, s.e.m.